Proteins containing photosynthetic reaction centre domains modulate FtsZ-based archaeal cell division

Phillip Nußbaum[1], Danguole Kureisaite-Ciziene[2], Dom Bellini [2],
Chris van der Does[1], Marko Kojic[3], Najwa Taib[4,5], Anna Yeates[2], Maxime Tourte[1],
Simonetta Gribaldo [4], Martin Loose [3], Jan Löwe [2]
& Sonja-Verena Albers [1,6] ✉

Cell division in all domains of life requires the orchestration of many proteins, but in Archaea most of the machinery remains poorly characterized. Here we investigate the FtsZ-based cell division mechanism in *Haloferax volcanii* and find proteins containing photosynthetic reaction centre (PRC) barrel domains that play an essential role in archaeal cell division. We rename these proteins cell division protein B 1 (CdpB1) and CdpB2. Depletions and deletions in their respective genes cause severe cell division defects, generating drastically enlarged cells. Fluorescence microscopy of tagged FtsZ1, FtsZ2 and SepF in CdpB1 and CdpB2 mutant strains revealed an unusually disordered divisome that is not organized into a distinct ring-like structure. Biochemical analysis shows that SepF forms a tripartite complex with CdpB1/2 and crystal structures suggest that these two proteins might form filaments, possibly aligning SepF and the FtsZ2 ring during cell division. Overall our results indicate that PRC-domain proteins play essential roles in FtsZ-based cell division in Archaea.

Cell division is a critical biological process in which cells reproduce and transmit their genetic material to their offspring. This process is facilitated by various proteins in different organisms. In bacteria, the FtsZ protein is essential for division[1], whereas eukaryotic cells use the ESCRT-III (Endosomal Sorting Complex Required for Transport) system[2]. Interestingly, in Archaea, both FtsZ- and ESCRT-based cell division systems exist[3,4]. Current knowledge about the archaeal FtsZ-based cell division system is limited, and only two proteins similar to bacterial counterparts have been characterized[4]: the GTP-dependent FtsZ[5–8] and a homologue of the FtsZ membrane anchor, SepF[7,8]. Archaea, such as the model organism *Haloferax volcanii*, often have two phylogenetically distinct FtsZ proteins[4]. These proteins, FtsZ1 and FtsZ2, play distinct roles in cell division, with FtsZ1 acting as a recruiting hub for other proteins and FtsZ2 being involved in the constriction process of the divisome[6]. Unusually, deletion mutants of the two *ftsZ* genes were possible, causing severe cell division defects, but the cells remained viable[6].

In Archaea, the membrane anchor for the cell division protein FtsZ has been identified as SepF, which is universally present alongside FtsZ in these organisms[7]. Although SepF is essential and the sole known FtsZ membrane anchor in Archaea, it interacts specifically with only one of the two FtsZ homologues, FtsZ2 (ref. [8]). How FtsZ1 is attached to the membrane is unknown, suggesting at a potentially undiscovered anchor. However, SepF's correct placement at the division site is reliant on FtsZ1, although no direct interaction between SepF and FtsZ1 has been observed and, unlike its bacterial counterpart, archaeal SepF does not polymerize[7,8].

To uncover additional proteins involved in archaeal cell division, co-immunoprecipitation experiments with SepF in *H. volcanii* were conducted[8], revealing two proteins with a photosynthetic reaction centre (PRC) barrel domain, a structural motif common across life forms that is involved in various cellular functions[9]. The PRC-barrel proteins found in Euryarchaeota are small and exclusively composed of this domain[9].

In this article, we show that two of the three identified PRC-barrel proteins play crucial roles in the FtsZ-based cell division of *H. volcanii*. Both CdpB1 (essential) and CdpB2 (not essential) notably affect cell division when mutated. These mutations also disrupt the typical localization of FtsZ and SepF proteins, indicating their integral role in the division process. Moreover, CdpB1 and CdpB2 were found to form a complex with SepF, with CdpB1 directly interacting with it. A combination of crystal structure determination of the CdpB1/B2 heterodimer, AlphaFold2 predictions and cryogenic electron microscopy (cryo-EM) showed CdpB1/B2 heterodimers that chain into alternating filaments with SepF dimers binding to CdpB1 dimers. These findings suggest CdpB1/B2 is involved in the inclusion of the membrane anchor SepF into a membrane-proximal polymer, one role of which is to localize FtsZ2 filaments to the division site.

Results

PRC-barrel proteins localize to the site of cell division

In *H. volcanii*, three PRC-barrel-domain-containing proteins were identified following immunoprecipitation experiments using the cell division protein SepF[8] and subsequent BLAST searches. These proteins, located at different genomic sites (*hvo_1691*, *hvo_1964* and *hvo_2019*), are not part of operons or neighbouring cell-division-related genes (Supplementary Fig. 1a). Averaging 10 kDa in size, these proteins are solely composed of PRC-barrel domains with conserved residues (Supplementary Fig. 1b).

We examined the cellular localizations of these proteins to understand their potential roles in cell division. These proteins, tagged with mNeonGreen and expressed under native promoters, showed distinct localization patterns. HVO_1691 prominently localized at the cell centre with additional peripheral foci, possibly due to overexpression (Fig. 1a). HVO_1964 was also clearly localized at the cell division site (Fig. 1c), whereas HVO_2019, not found in the SepF immunoprecipitation[8], displayed a diffuse pattern throughout the cytoplasm with faint mid-cell localization (Supplementary Fig. 2a). Owing to their localization pattern at the site of cell division, we named these proteins cell division proteins B1 (CdpB1; HVO_1691), CdpB2 (HVO_1964) and CdpB3 (hvo_2019). Despite partial cleavage from the fluorescence tag, as confirmed by western blotting, the localization patterns of each CdpB protein are believed to be accurate because mNeonGreen alone does not localize in this pattern (Supplementary Fig. 3a,b). These findings suggest distinct roles for the CdpB proteins in the cell division process, with particular emphasis on the involvement of CdpB1 and CdpB2 at the division site.

We then observed the co-localization of these proteins with the SepF protein. CdpB1–mCherry strongly overlapped with SepF–smRS-GFP (Fig. 1b), whereas CdpB2–mCherry's signal was broader yet still centred in the cell (Fig. 1d). The CdpB3–mCherry signal intensity was the highest at the cell centre, overlapping with the SepF signal, but also showed cytoplasmic distribution as previously observed (Supplementary Fig. 2b). When CdpB proteins were compared with each other, CdpB1 and CdpB2 showed substantial overlap at the cell centre (Supplementary Fig. 2d), indicating a shared role during division. CdpB3's diffuse pattern only coincided with the other proteins at the division site (Supplementary Fig. 2e,f).

Live-cell imaging showed that CdpB1 and CdpB2 consistently localized at the cell centre throughout the cell cycle and relocated to the future division site in daughter cells (Fig. 1e and Supplementary Videos 1 and 2). The CdpB1 foci mentioned above were not obviously involved in the cell division process but increased in intensity over time, supporting our suspicion that these might be protein aggregates rather than functional proteins. CdpB3's signal intensified at the division site just before constriction and was less defined elsewhere during the cycle (Supplementary Fig. 2c and Supplementary Video 3). These observations collectively imply that all three CdpB proteins, with their PRC domains, are integral to the cell division machinery in *H. volcanii*.

Mutations of CdpB1 and CdpB2 have strong effects on cells

To understand the specific functions of CdpB proteins in *H. volcanii*, we attempted to delete their genes. Although *cdpB1* proved essential, indicating a critical role in cell division, we successfully created a conditional depletion strain by replacing its native promoter with a tryptophan-inducible one (HTQ275), a technique previously applied to the essential protein SepF[8]. However, this promoter failed to produce sufficient CdpB1 levels to completely restore the wild-type phenotype (Supplementary Fig. 4a). Upon CdpB1 depletion, cells became filamentous or enlarged with irregular shapes compared with wild type (Fig. 2a and Supplementary Videos 4 and 5), a condition resembling the effects seen with the deletion of FtsZ1, FtsZ2 or SepF[6,8]. This morphological change was accompanied by a broader distribution of FtsZ1, FtsZ2 and SepF, suggesting CdpB1's role in defining a precise division site (Fig. 2c and Supplementary Table 1). Moreover, multiple division sites were visible in filamentous HTQ275 cells. Those cells, harbouring plasmids, were less irregular (Fig. 2b and Supplementary Fig. 5a), hinting at the influence of plasmids on cell shape, potentially due to the auxotrophic selection markers used in *H. volcanii* genetics as recently described[10]. We also assessed the functionality of the CdpB1–mNeonGreen fusion protein using HTQ275. Although this fusion protein restored cell viability to wild-type levels, it failed to correct the cell size anomaly (Supplementary Fig. 6a–c). Expressing CdpB1 without a tag from a plasmid controlled by its native promoter similarly restored viability but not the elongated cell shape (Supplementary Fig. 7a–c).

In contrast to CdpB1, it was possible to obtain a *cdpB2*-knockout strain, HTQ272, and its cells showed reduced viability compared with wild type (Supplementary Fig. 4b). Unlike the typical rod-to-plate transition observed in wild-type cells[11], CdpB2-deficient cells were filamentous and became extremely enlarged by the end of the exponential phase (Fig. 2d). We quantified these shape changes by measuring cell area due to their varied morphologies (Supplementary Fig. 5b and Supplementary Table 2). In addition, localization studies of other cell division proteins in HTQ272 revealed broader distributions of SepF, FtsZ1 and FtsZ2 at the cell centre, but the distributions were not as dispersed as in the CdpB1 depletion strain (Fig. 2e and Supplementary Table 1). However, these cells also became filamentous due to the presence of the expression plasmids, with several sites of cell division. Also, expression of CdpB2–mNeonGreen in HTQ272 restored viability but not cell shape (Supplementary Fig. 6d–f). In contrast, tag-less expression of CdpB2 from a plasmid under the control of its native promotor restored both viability and cell morphology (Supplementary Fig. 7a–c).

Finally, we created HTQ271, a *cdpB3* deletion strain that showed no notable changes in viability (Supplementary Fig. 4b), cell shape (Supplementary Fig. 5c and Supplementary Table 2) or localization of FtsZ1, FtsZ2 or SepF compared with wild type (Supplementary Fig. 8a,b and Supplementary Table 1). HTQ271 and wild-type cells both transitioned from rod shaped to plate shaped during growth, with division proteins forming a defined ring at the cell centre. The *cdpB2* and *cdpB3* double-deletion strain, HTQ273, showed growth, cell shape and protein localization phenotypes similar to the *cdpB2* single-deletion strain (Supplementary Figs. 4b, 5d, and 8c,d, and Supplementary Tables 1 and 2). Overall these observations indicate CdpB3's limited impact on *H. volcanii*'s cell division machinery. For an overview of the signal areas of the three labelled cell division proteins in the *cdpB* deletion or
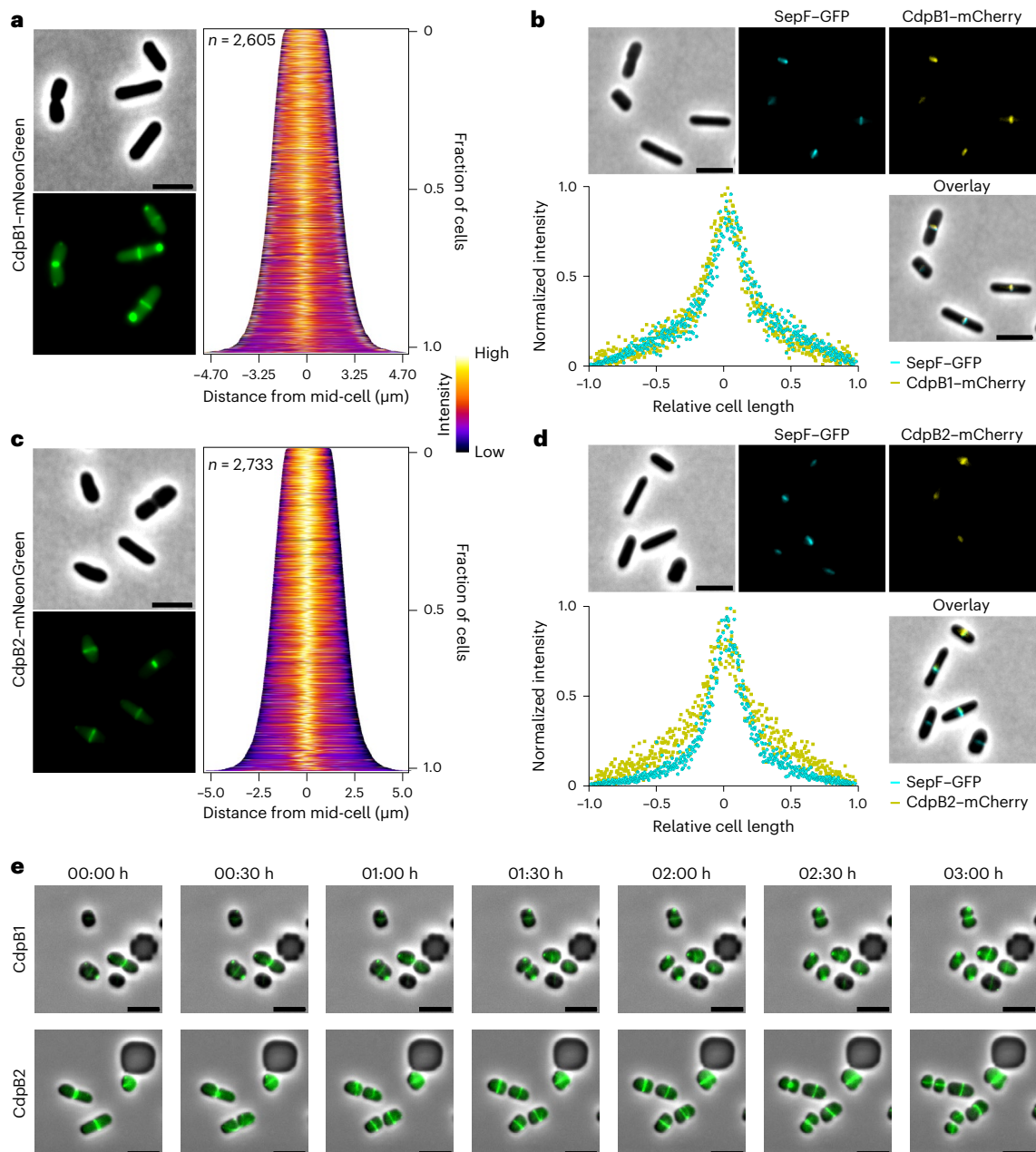
Fig. 1 | Cellular positioning of PRC-barrel proteins CdpB1 and CdpB2 and their co-localization with divisome protein SepF. a, Fluorescence microscopy of cells in the early exponential phase expressing CdpB1–mNeonGreen under control of the native *cdpB1* promotor. Demographic analysis shows that the highest signal intensity is at the cell centre, together with some polar foci. **b**, Co-localization of SepF–GFP with CdpB1–mCherry in cells during the early exponential phase. The intensity profiles of normalized SepF–GFP (cyan) and CdpB1–mCherry (yellow) show strong overlap. **c**, Fluorescence microscopy of cells in the early exponential phase expressing CdpB2–mNeonGreen under control of the native *cdpB2* promotor. Demographic analysis shows that the highest signal intensity is at the cell centre, together with some polar foci. **d**, Co-localization of SepF–GFP together with CdpB2–mCherry in cells during the early exponential phase. The intensity profiles of normalized SepF–GFP (cyan) and CdpB2–mCherry (yellow) show a broader localization for CdpB2. All localization experiments were performed in 3 independent replicates, with >1,000 cells used in total for analysis. **e**, Time-lapse microscopy of cells expressing CdpB1–mNeonGreen or CdpB2–mNeonGreen under control of their native promotors in microfluidic chambers. Videos were recorded for 16 h, and a selection of 3 h of the videos is shown. For each construct, at least three independent videos were recorded, showing essentially the same results. Scale bars, 4 μm.

depletion strains, see Supplementary Fig. 8e; the mean areas are listed in Supplementary Table 1.

Positioning of CdpB proteins depends on other cell division proteins

To delve deeper into the roles of CdpB proteins and their interplay with other division proteins, we observed their localization in the absence of SepF, FtsZ1 or FtsZ2. In the SepF depletion strain HTQ239 (ref. 8), before any depletion effects, CdpB1 and CdpB2 showed normal localization

(Fig. 3a,b). As SepF depletion progressed, cells became filamentous and, after 6 h, CdpB1's ring-like structures began to fade whereas CdpB2 maintained some localization at division sites. After 24 h, only scattered foci of CdpB1 and CdpB2 were seen, in contrast to their defined ring structures in control cells (Fig. 3a,b). CdpB3, initially faint at the cell centre, diffused throughout the cytoplasm without forming foci upon SepF depletion (Supplementary Fig. 9a).

In an *ftsZ1* deletion strain, we observed enlarged, rough cells with CdpB1 and CdpB2 diffusely located, forming scattered foci, showing
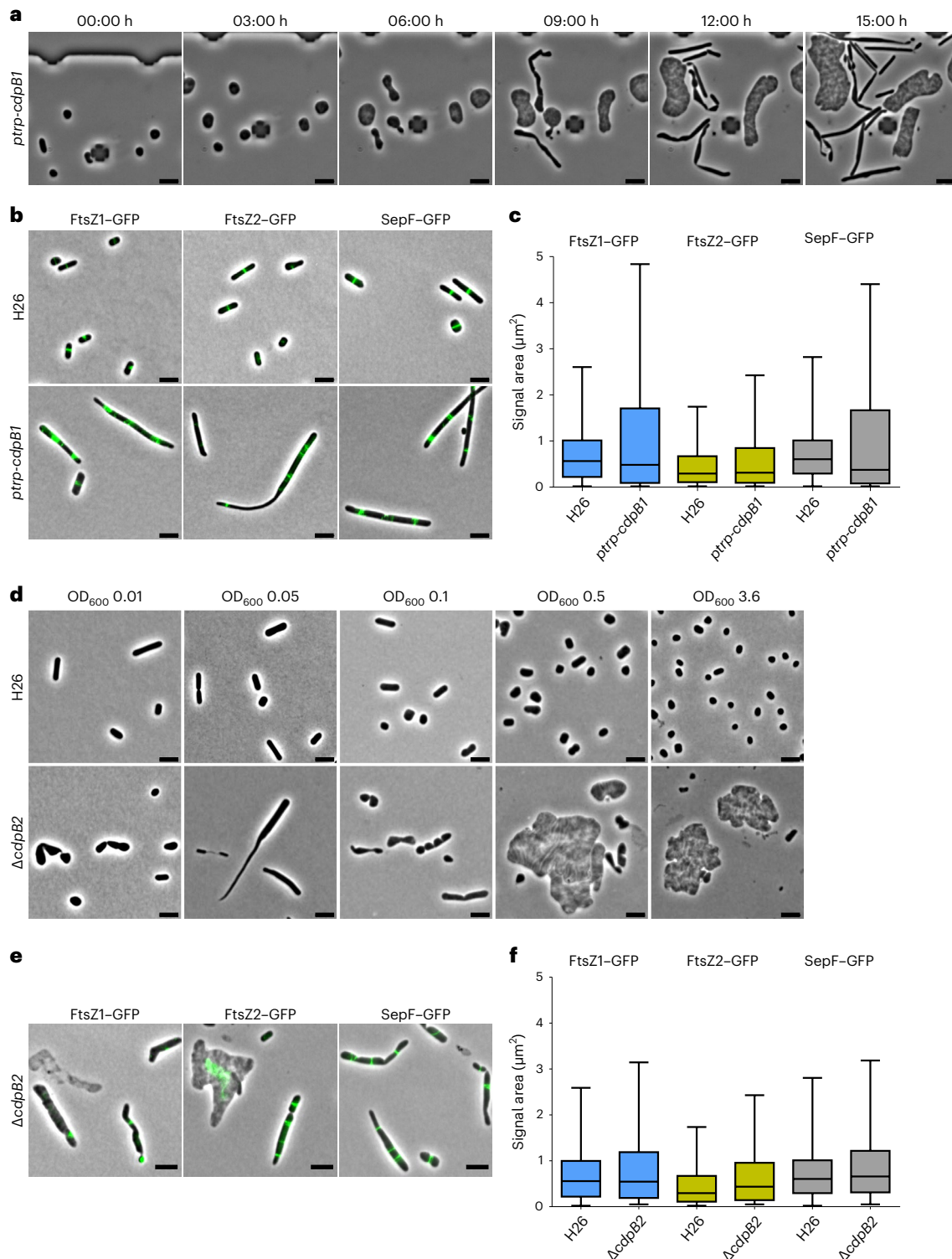
Fig. 2 | Effect of CdpB1 depletion and CdpB2 deletion on cell shape and the positioning of cell division proteins. a, Time-lapse microscopy of *ptrp-cdpB1* (HTQ275) cells under CdpB1 depletion conditions in a microfluidic chamber. Only part of the 15 h video is shown. Three independent videos were recorded showing essentially the same results. b, Fluorescence microscopy of wild-type cells (H26) and CdpB1-depleted cells (HTQ275) expressing GFP-tagged FtsZ1, FtsZ2 and SepF. c, Analysis of the signal area of each GFP construct in both strains. d, Microscopy of the wild-type (H26) and the *cdpB2* deletion strain (HTQ272) during different growth stages (OD$_{600}$, 0.01 lag phase, 0.05–0.5 exponential phase, 3.6 stationary phase). e, Fluorescence microscopy of the *cdpB2* deletion strain HTQ272 expressing GFP-tagged FtsZ1, FtsZ2 and SepF. f, Analysis of the signal area of each GFP construct in H26 and HTQ272. Signal areas in c and f are summarized in box plots; boxes extend from the 25th to the 75th percentile, the whiskers indicate the minimum and maximum values and the horizontal line indicates the median. The plots include data from 3 independent replicates per strain and GFP construct, with >1,000 cells being analysed in total. Scale bars, 4 µm.

FtsZ1 influences their positioning (Supplementary Fig. 9b). CdpB3 was, as in the SepF depletion strain, observed throughout the cells. The *ftsZ2* deletion strain showed filamentation and allowed clearer observation of CdpB proteins, which formed ring-like structures and occasional foci (Supplementary Fig. 9b). In contrast, cells from the *ftsZ1/Z2* double-deletion mutant were neither enlarged nor filamentous,
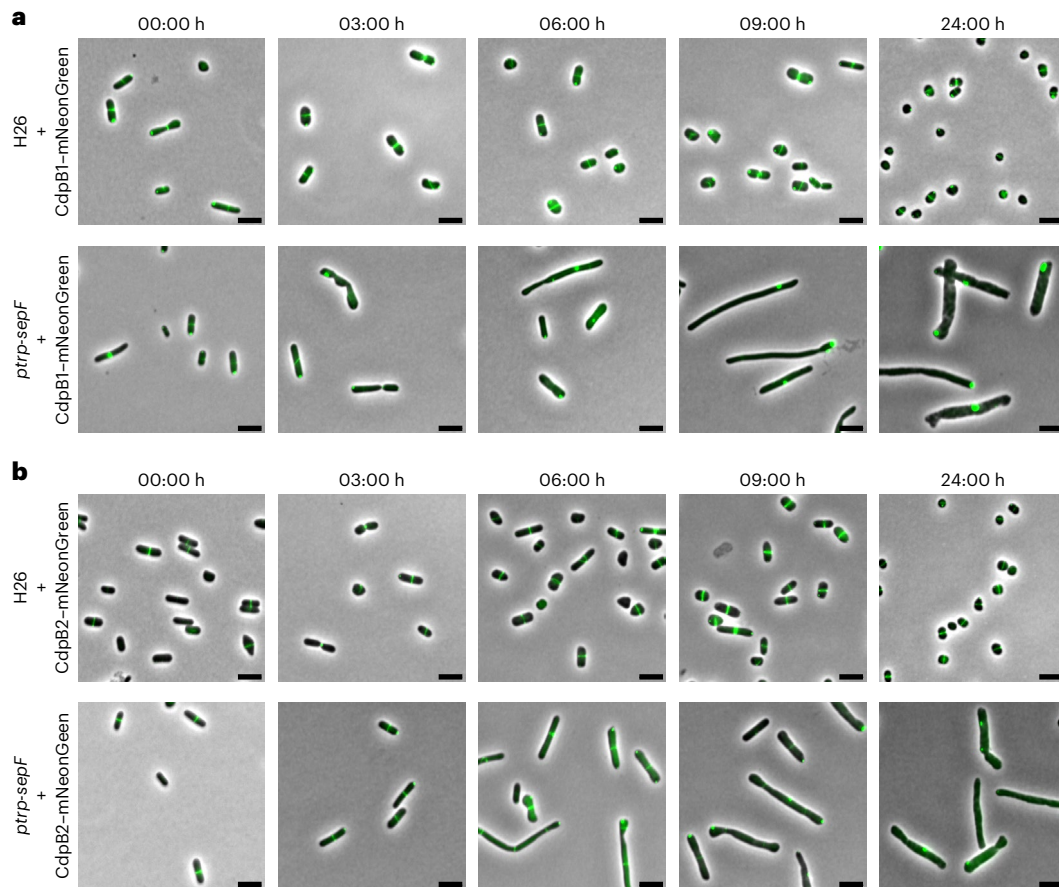
Fig. 3 | CdpB1 and CdpB2 localization during SepF depletion. a, Fluorescence microscopy of H26 and the SepF depletion strain HTQ239 expressing CdpB1–mNeonGreen from a plasmid under the control of its native promotor. **b**, Fluorescence microscopy of H26 and the SepF depletion strain HTQ239 expressing CdpB2–mNeonGreen from a plasmid under the control of its native promotor. Cells in **a** and **b** were imaged before (0 h) and at different time points after SepF depletion was induced. The experiments were repeated three times with essentially the same outcome. Scale bars, 4 μm.

displaying only CdpB1 foci and diffuse distribution of the other CdpB proteins (Supplementary Fig. 9b).

To explore interdependencies, we studied CdpB2 localization in the CdpB1 depletion strain and CdpB1 localization in the CdpB2 deletion strain. Results indicated that CdpB2's proper localization relies on CdpB1, but CdpB1 can form a ring-like structure independently of CdpB2 (Supplementary Fig. 9c,d).

These findings suggest a hierarchy in which CdpB1's positioning is influenced by SepF, whereas CdpB2's placement is contingent on CdpB1's correct localization, underscoring a complex interplay of cell division proteins in *H. volcanii*.

CdpB1 and CdpB2 together form a complex with SepF

The loss of CdpB1 and CdpB2 localization during SepF depletion and CdpB2's reliance on CdpB1 indicate an interdependency between SepF and CdpB proteins. To study their interactions, we used homologues from the hyperthermophilic archaeon *Archaeoglobus fulgidus* (CdpB1, 46.2% sequence identity to *H. volcanii*; CdpB2, 40.8% sequence identity; and SepF, 42% sequence identity; Supplementary Fig. 10f), which are more biochemically tractable than their highly salt-dependent *H. volcanii* counterparts. These homologues (CdpB1, CdpB2 and SepF) were heterologously expressed in *Escherichia coli*, purified and analysed via size exclusion chromatography (SEC). CdpB1 and SepF formed dimers independently, whereas CdpB2 remained monomeric. CdpB1 and SepF showed complex formation (Fig. 4a) but CdpB2 did not interact with SepF (Fig. 4b). Interestingly, CdpB1 and CdpB2 showed interaction (Fig. 4c), and all three proteins together formed a tripartite SepF–CdpB1–CdpB2 complex (Fig. 4d). Sodium dodecyl sulfate–polyacrylamide

gel electrophoresis (SDS–PAGE) of the peak elution fractions of the individual proteins and their complexes is shown in Supplementary Fig. 10a. Similar complex formations were also confirmed with *H. volcanii* proteins (Supplementary Fig. 10b–e), indicating conserved interactions and probably similar in vivo functions between the two species.

Crystal structure of the CdpB1 and CdpB2 heterodimer

To explore the interactions within the SepF–CdpB1–CdpB2 complex from *A. fulgidus*, we attempted crystallization but only succeeded with the CdpB1/B2 heterodimer. Crystals diffracted to a resolution of 2.3 Å were orthorhombic with space group $P2_12_12_1$ containing four heterodimers in the asymmetric unit. The structure was solved by molecular replacement using an AlphaFold2 model of CdpB1. Crystallographic and refinement statistics are summarized in Supplementary Table 3. For two heterodimers, residues 1–92 and 1–76 were built for CdpB1 and CdpB2, respectively. In the other two heterodimers, only residues 1–76 were visible in the electron density for both CdpB1 and CdpB2. All four heterodimers are very similar to each other and will be discussed together (Fig. 5a,b). The CdpB1/B2 heterodimer is built through pseudo-two-fold symmetry that relates the two PRC domains to each other. CdpB1 and CdpB2 are very similar in structure, including their (small) loop regions (Fig. 5c). They adopt near-identical all-β-folds, similar to *Methanobacterium thermoautotrophicum* MTH1859 (PDB: 1PM3)[12]. Briefly, their mainly antiparallel six-stranded β-sheet is heavily bent to form a U structure, with the two halves of the sheet connected through strand β3 and sandwiched onto each other (Fig. 5b). The head-to-head dimerization interface mainly comprises strands β3 and β4 symmetrically crossing over between the two subunits. A short
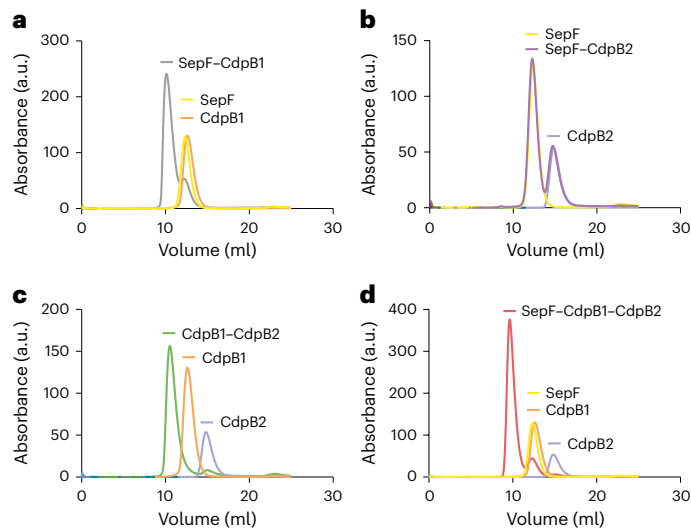
Fig. 4 | Biochemical analysis of CdpB1, CdpB2 and SepF from *A. fulgidus*.
a–**d**, SEC to investigate complex formation: SepF (yellow) and CdpB1 (orange) alone and SepF–CdpB1 together (grey) (**a**); SepF (yellow) and CdpB2 (blue) alone and SepF–CdpB2 together (purple) (**b**); CdpB1 (orange) and CdpB2 (blue) alone and CdpB1–CdpB2 together (green) (**c**); and SepF (yellow), CdpB1 (orange), and CdpB2 (blue) alone and SepF–CdpB1–CdpB2 together (red) (**d**).

strand, β1, followed by a short one-turn α-helix, α1, extends the β-sheet of the partner subunit by packing in an antiparallel manner against the carboxy (C) terminus of β3, reinforcing the dimerization interface (Fig. 5a,b). Mutations introduced at the dimerization interface of CdpB1 (V39E) and CdpB2 (L37E) (Supplementary Fig. 11c) revealed distinct effects on cellular localization. Although mutated CdpB1 retained its ring-like structure at the cell centre, resembling wild-type behaviour (Supplementary Fig. 11a), mutated CdpB2 lost its mid-cell localization, becoming diffusely distributed (Supplementary Fig. 11b), underscoring the dependency of CdpB2 on direct interaction with CdpB1 for proper positioning. Western blot analysis confirmed the integrity of the mutated fusion proteins, validating the observed localization changes as consequences of disrupted dimerization rather than protein degradation (Supplementary Fig. 11d).

CdpB1 and CdpB2 form filaments that bind SepF
Inspection of the crystal packing revealed that there are also homotypic interactions present, both for CdpB1–CdpB1 and for CdpB2–CdpB2, and that they use two-fold symmetry in very similar ways (Fig. 5d). This arrangement of pseudo-two-fold CdpB1–CdpB2 heterodimers and two-fold CdpB1–CdpB1 and CdpB2–CdpB2 homodimers creates open-ended symmetry, meaning a polymer or a filament. However, the crystals do not contain very long filaments because the filament is bent in one direction (Fig. 5e). As crystal symmetry is used to form the filament, the filaments cannot extend all the way through the orthorhombic lattice of the crystals. AlphaFold2 predictions using CdpB1 or CdpB2 monomers reproduce the crystal structure almost perfectly, and reveal the same heterodimer as revealed experimentally with high precision. Given more CdpB1 and CdpB2 monomers, AlphaFold2 predicts the same alternating polymer as the one revealed in the crystal packing (Fig. 5d versus 5f). Given the above we think it is highly likely that CdpB1 and CdpB2 form alternating filaments of heterodimers. Owing to the failure in revealing the tripartite SepF–CdpB1–CdpB2 complex by crystallography, we used cryo-EM to gain further insights. The complex formed dispersed single particles, whose structure we could resolve to a resolution of 5.1 Å by cryo-EM. The tripartite complex contained dimers of CdpB2–CdpB1–CdpB1–CdpB2, with two SepF dimers close to the two pairs of CdpB1 (Fig. 5g, left). Inspection revealed that each CdpB2–CdpB1–CdpB1–CdpB2 stretch (coloured blue and orange in

Fig. 5g, right) is identical to a stretch of the CdpB1–CdpB2 polymer found by crystallography and AlphaFold2 (Fig. 5e). Further inspection revealed that the dimeric assembly is also present in the crystal packing previously described, so it also seems to be a conserved mode of interaction. The precise interaction of SepF with CdpB1 could not be revealed by cryo-EM because of the low resolution, although tubular densities on the outside of CdpB1 subunits (visible in Fig. 5g, left) hinted at SepF tails clamping around the CdpB1 dimer on the outside. To gain more insights, we again turned to AlphaFold2 to predict the structure of the tripartite complex of CdpB1/B2 with SepF. For this we used several copies of each protein because we showed that CdpB1–CdpB2 is likely to polymerize and SepF is known to form dimers. The resulting prediction (Fig. 5h) revealed the aforementioned CdpB1–CdpB2 alternating filament, with SepF dimers bound to CdpB1 dimers, as indicated by the cryo-EM structure (Fig. 5g, left). The amino-terminal (N-terminal) aliphatic helix of SepF that is predicted to bind to the cell membrane is located on the concave side of the CdpB1–CdpB2 filament, whereas SepF's C-terminal globular domain forms the expected dimer on the convex side of the filament. To show that the tripartite SepF–CdpB1–CdpB2 complex indeed binds to the membrane, we performed liposome-binding experiments that we imaged by cryo-EM (Fig. 5i). Liposomes made from *Pyrococcus* lipid extract failed to bind SepF alone (Fig 5i, top left) and became somewhat decorated with SepF–CdpB1 (Fig. 5i, top right), whereas addition of the tripartite complex led to almost complete coverage of the membrane (Fig. 5i, bottom). Similarly, pelleting assays using the proteins from *H. volcanii* in the presence of multi-lamellar vesicles also showed that SepF anchors the SepF–CdpB1–CdpB2 complex to the membrane (Supplementary Fig. 12a). Moreover, the interaction of SepF with FtsZ2 and the ability of SepF to anchor FtsZ2 to the membrane (Supplementary Fig. 12b) was not negatively affected by the presence of CdpB1 (Supplementary Fig. 12c). It is worth noting that previous studies have shown that the FtsZ tail binds to the C-terminal SepF dimer[7,13,14], and a model would hence predict that FtsZ filaments are located on the convex side, which is facing the cytoplasm. We also note that previous structures of PRC-barrel proteins have also revealed filaments in their crystal packings, consisting in these cases of only one type of subunit (Fig. 5j). To endorse our claim that CdpB1 and CdpB2 polymerize, we performed mass photometric analysis of the two proteins from *H. volcanii*. The proteins were either analysed independently from each other, each with a mass of around 75 kDa, or the proteins were combined, which shifted the measured mass to 119 kDa (Supplementary Fig. 12d). As the calculated molecular weight of a CdpB1 monomer is 10.8 kDa and that of a CdpB2 monomer is 9.0 kDa, this shift in mass supports the formation of a co-polymer.

PRC-barrel-containing proteins are widespread in Archaea
PRC-barrel-domain-containing proteins, part of a large family, are widespread in Archaea, as revealed by screening 3,661 archaeal genomes for PRC and CdvA domains using the pfam domain PF05239 (PRC) and PF18822 (CdvA), which share similarity with the PRC-barrel proteins[9]. Present in all Euryarchaeota, DPANN-superphylum (Aenigmatarchaeia, Diapherotrites, Huberarchaeia, Micrarchaeia, Nanoarchaeia, Nanohaloarchaeia, Undinarchaeia), Asgardarchaea and TACK-superphylum (Bathyarchaeia, Thermoproteia/Crenarchaeota, Korarchaeia, Nitrososphaeria/Thaumarchaeota, Verstraetearchaeota) groups (Supplementary Fig. 13; see source data in Supplementary Data 1), their distribution aligns with that of FtsZ and SepF, suggesting a functional connection. However, CdvA homologues are only found in Asgardarchaea and TACK supergroups. Whereas most archaeal classes have fewer than three PRC copies, Methanobacteria average five (Supplementary Fig. 13; see source data in Supplementary Data 1). Typically, sequences contain either a singular PRC or CdvA domain, with these 'stand-alone' proteins appearing across all archaeal groups. Few PRC proteins are associated with other domains such as a zinc ribbon. Intriguingly, although some absences can be due to incompleteness of metagenome-assembled
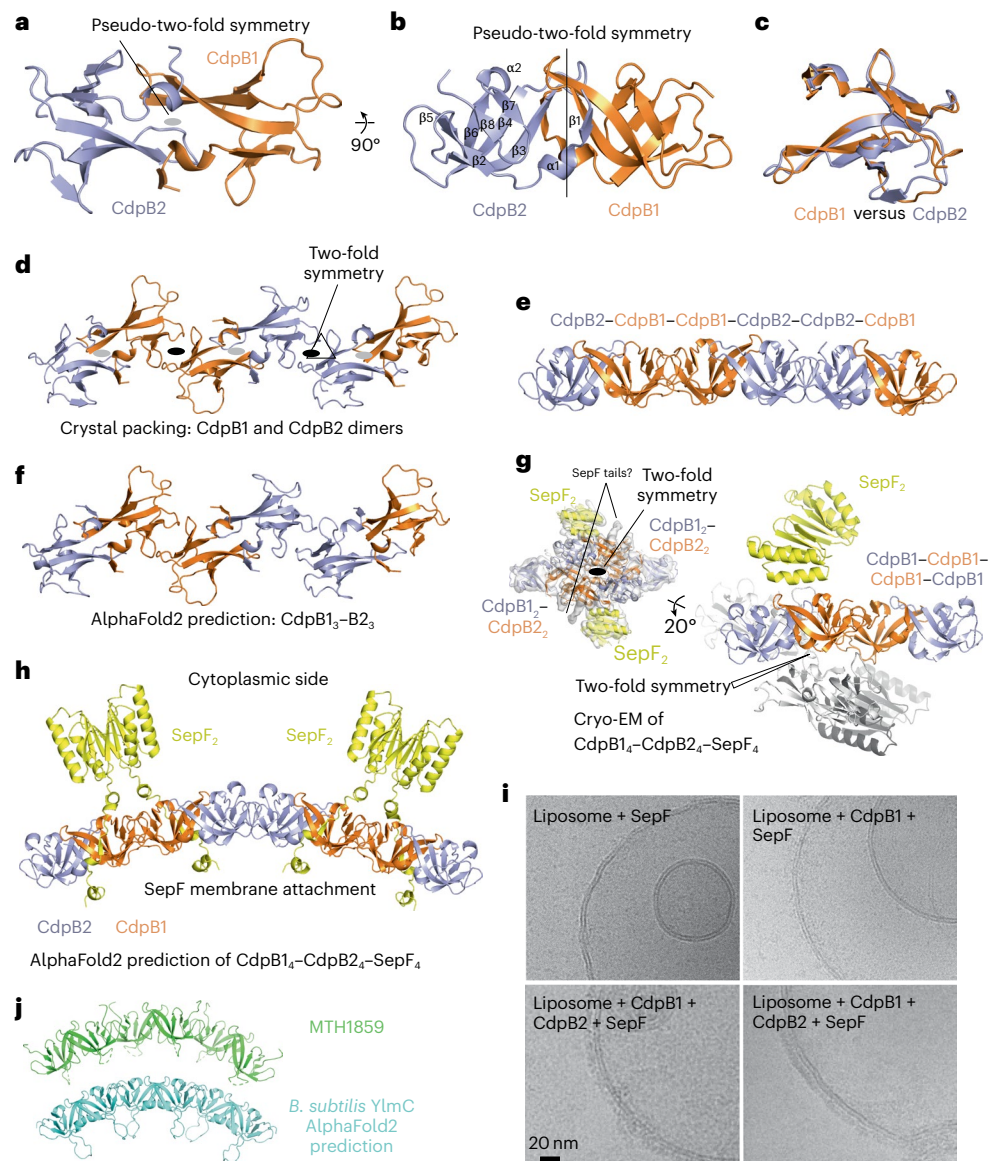
Fig. 5 | Crystal structure of the CdpB1–CdpB2 complex and cryo-EM with SepF and liposomes. a, Crystal structure of the CdpB1 (orange) and the CdpB2 (blue) heterodimer at a 2.3 Å resolution (top view showing the pseudo-two-fold symmetry axis). **b**, CdpB1–CdpB2 structure side view. **c**, Superposition of the CdpB1 and CdpB2 monomers showing their strong similarity. **d**, Crystal packing of the CdpB1 and CdpB2 homodimers, revealing alternating filaments of CdpB1 and CdpB2 homo- and heterodimers (top view, same as in **a**). **e**, Same as in **d**, but a side view revealing a slight bend (side view same as in **b**). **f**, AlphaFold2 predicts the same alternating filament of CdpB1–CdpB2. **g**, Cryo-EM structure at a 5.1 Å resolution of the tripartite CdpB1–CdpB2–SepF complex (left, with map superimposed). A dimer is revealed that contains a CdpB2–CdpB1–SepF–SepF–CdpB1–CdpB2 complex. Right: SepF is located above the CdpB1 dimer of the CdpB2–CdpB1–CdpB1–CdpB2 stretch that is identical to part of the filament in the crystals as shown in **d** and **e**. **h**, AlphaFold2 predicts a very similar arrangement of the CdpB1–CdpB2–SepF complex, but also predicts the CdpB2–CdpB2 contact that is absent in the cryo-EM structure and that leads to filament formation. SepF's N-terminal amphipathic helix is located at the concave side of the filament, whereas the FtsZ-binding dimeric C-terminal SepF domain is on the convex side, which is presumed to face the cytoplasm of the cell, where FtsZ would be located. **i**, Cryo-EM of liposomes with CdpB1/B2 and SepF samples reveals that complete liposome coating requires all three proteins to be present and is supportive of the idea that the filament shown in **h** is formed on the membrane. Exemplary images of three independent repetitions are shown. **j**, Previous crystal structure of putative adaptor protein MTH1859 from *M. thermoautotrophicum* (green, top) and AlphaFold2 prediction of YlmC from *B. subtilis* (cyan, bottom). Both reveal an analogous homomeric filament to the one formed by CdpB1–CdpB2 and shown in **d**–**f**.

genomes of uncultured lineages, very few PRC-domain-containing proteins were found in the 69 analysed genomes of Lokiarchaeia, unlike other Asgardarchaea groups (Heimdallarchaeia and Thorarchaeia), where at least one PRC protein was found (Supplementary Fig. 13; see source data in Supplementary Data 1).

Discussion

The initial hint of PRC-barrel-domain-containing proteins' involvement in archaeal cell division emerged from studying the genome of an uncultured member of the phylum Korarchaeota. This organism has a gene cluster featuring a PRC-barrel-domain gene and multiple *ftsZ* paralogues[15]. Our research indicates that two PRC-barrel-domain proteins are actually involved in, and are partially essential for, FtsZ-based cell division in Archaea, whereas the third homologue (CdpB3), although localized at the site of cell division, showed no apparent phenotype when mutated.

CdpB1 and CdpB2 help form a distinct cell division plane, organizing FtsZ1, FtsZ2 and SepF into a cytokinetic ring. CdpB1 directly
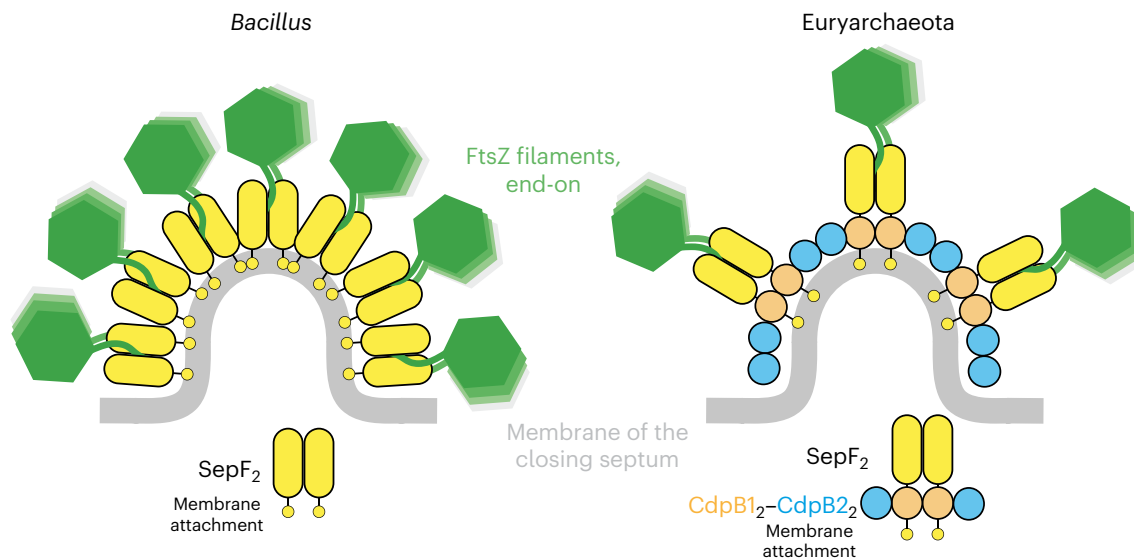
Fig. 6 | Model for CdpB1/B2 function in Euryarchaeota. Left: in bacteria such as *B. subtilis*, SepF dimers (yellow) polymerize into bent filaments. It has been postulated that the curvature of the SepF filaments is used to restrict the width of the nascent septum[17], which in *Bacillus* forms a cross-wall. In *Bacillus*, SepF also functions as an alternative FtsZ membrane anchor, in addition to FtsA, attaching FtsZ polymers (green, running orthogonal to the two-dimensional plane) to the cell membrane. Right: euryarchaeal SepFs have not been shown to polymerize, which is probably due to the absence of the glycine that would be equivalent to *Bacillus* SepF G109, which is important for polymer formation. Instead, we show here that alternating units of CdpB1 (orange) and CdpB2 (blue) dimers are able to form alternating heteropolymers. We also show that SepF binds to CdpB1, which, taking the AlphaFold2 model in Fig. 4k into consideration, means that the CdpB1–CdpB2 polymer is probably attached to the cell membrane on the concave side, and to FtsZ filaments on the convex side that faces the cytoplasm. An overall arrangement analogous to the one postulated for *B. subtilis* SepF polymers emerges and it can be speculated that the CdpB1–CdpB2–SepF polymer might restrict cell constriction width in similar ways as in *B. subtilis*.

interacts with SepF and CdpB2, forming a tripartite complex that, based on our data, probably creates a filament of alternating CdpB1 and CdpB2 dimers. Archaeal SepF dimers have been shown to not polymerize[7,8], most probably due to the absence of the conserved G109, which was shown to be crucial for polymerization of *Bacillus subtilis* SepF dimers[16]. Bacterial SepF is associated with membrane curvature sensing and possibly membrane remodelling that requires the aforementioned polymerization of SepF dimers into oligomeric states[14,16]. This CdpB1/B2 filament, along with archaeal SepF dimers, might support membrane activities similarly to bacterial systems, rendering archaeal SepF polymerization unnecessary (Fig. 6). Indeed, the intrinsic curvature of the CdpB1/B2 filaments resemble that of bacterial SepF polymers, at least in their direction, with negative curvature facing the membrane[14,16]. As CdpB1/B2 mutants showed wider FtsZ1/Z2 and SepF localization, we suggest that CdpB1–CdpB2–SepF polymers restrict the width of the cell constriction similar to *B. subtilis*[16,17] (Fig. 6). Despite this intriguing model, it should be mentioned that a slight impact on vesicles by archaeal SepF dimers from *Methanobrevibacter smithii* has also been reported[7]. However, verifying this model requires studying the full complex, including archaeal FtsZ homologues. So far, we obtained biochemical evidence of an interaction between SepF and FtsZ2 from *H. volcanii* in vitro, suggesting that SepF anchors FtsZ2 to the membrane and is not negatively affected by additional binding of CdpB1.

In *H. volcanii*, the divisome assembly involves interdependent localization of FtsZ1, FtsZ2 and SepF[6,8]. The exact order of the process is unclear, varying between the hierarchical structure seen in *E. coli*[18] and the dynamic assembly in *B. subtilis*[19]. FtsZ1 is important at the division site, acting as a platform for other proteins, with SepF's placement dependent on FtsZ1 and FtsZ2's localization reliant on SepF[6,8]. We showed that CdpB1 and CdpB2's ring formation at the division site requires SepF, with CdpB2's placement directly affected by CdpB1's presence. However, absence of CdpB1 and CdpB2 disrupts the entire cell division machinery, leading to disorganized FtsZ1, FtsZ2, and SepF and enlarged cell sizes due to disrupted S-layer protein incorporation, which is synthesized at the site of cell division[20]. This suggests a relaxed hierarchy in the divisome assembly of *H. volcanii*, resembling the dynamic assembly of *B. subtilis* more than the strict linear order of assembly in *E. coli*.

Interestingly, PRC-barrel-domain proteins are crucial in archaeal cell division, not just for the FtsZ-based mechanism. The essential CdvA protein, involved in ESCRT-III-based division[21], contains an N-terminal PRC-barrel domain[22,23].

In conclusion, we show that the PRC barrel is an essential protein domain in archaeal cell division that is important for the organization of the other cell division proteins into functional cell division machinery. In accordance with this, a recent publication also investigating the PRC-domain proteins in *H. volcanii* supports some of our findings[24], confirming the newly assigned function of PRC-barrel-domain-containing proteins as important players in archaeal cell division that is based on the FtsZ system.

Methods

If not stated otherwise, all chemicals were either purchased from Roth or Sigma.

Strains and growth media

E. coli cells for cloning and protein production were grown in lysogeny broth (LB) liquid medium or on LB-agarose plates[25] supplemented with required antibiotics. Depending on the selection marker, either ampicillin (100 μg ml⁻¹) or kanamycin (25 μg ml⁻¹) was used. Cells were grown at 37 °C and liquid cultures were shaken at 150 rpm. *H. volcanii* cells were grown in full YPC medium (5 g l⁻¹ yeast extract (Oxoid), 1 g l⁻¹ Peptone (Oxoid) and 1 g l⁻¹ Bacto Casamino Acids (BD Biosciences)), pH adjusted to 7.2 with KOH[26], or selective Casamino acids medium (5 g l⁻¹ Bacto Casamino Acids; BD Biosciences), pH adjusted to 7.2 with KOH[26], supplemented with an extended trace element solution (Cab medium: Ca medium + trace elements)[27]. If necessary, the selective medium was supplemented with 0.45 mM uracil. Liquid cultures smaller than 5 ml were grown in 15 ml tubes under constant rotation at 45 °C. Larger cultures

were grown in flasks under constant shaking (120 rpm) at 45 °C. Plates to grow *H. volcanii* transformants were prepared as previously described[26]. To prevent evaporation, plates were incubated in plastic containers at 45 °C. The strains used in this study are listed in Supplementary Table 4.

Plasmid construction

Plasmids were either cloned via restriction-enzyme-based cloning or by in vivo ligation[28]. All enzymes for DNA amplification (Phusion Polymerase) and plasmid construction (restriction enzymes, T4 DNA ligase and Quick CIP) were obtained from New England Biolabs (NEB) and used according to the manufacturer's protocol. Plasmids for the expression of fluorescently tagged proteins were constructed via restriction-enzyme-based cloning. For the knockout plasmids, around 500 bp of the upstream region and around 500 bp of the downstream region of the respective *cdpB* genes were amplified. The two fragments were connected via a BamHI restriction site and the ligated product cloned into linearized pTA131 (ref. 26) by in vivo ligation using 17 bp of homologous regions per site. For the *cdpB1* depletion plasmid, *cdpB1* was cloned into pTA1369 (ref. 29) to have the tryptophan-inducible promotor in front of the gene. The complete cassette of *ptnA1-cdpB1* and an *hdrB* selection marker was then cut out from the plasmid with BglII and cloned in between the up- and downstream region of the *cdpB1*-knockout plasmid, opened with BamHI. Plasmids for the heterologous expression of CdpB1, CdpB2 and SepF from *A. fulgidus* were constructed with in vivo ligation. The genes were ordered codon optimized from GenScript and amplified with 15 bp overhangs complementary, per site, to the linearized His−SUMO expression plasmid pSVA13429. Cell division proteins of *H. volcanii* for heterologous protein expression were also cloned in expression plasmid pSVA13429 as previously described. Plasmids for the expression of point-mutated CdpB1 and CdpB2 fused to mNeonGreen were created by linearization of the same plasmids used for CdpB1 and CdpB2 localization, with the mutation inserted via the forward primer. The linearized plasmids were circularized by treatment with T4 polynucleotide kinase (NEB) and subsequently T4 DNA ligase (NEB) according to the manufacturer's protocol. All plasmids, primers and enzymes used in this study are listed in Supplementary Tables 5 and 6. A table with gene sequences and the respective protein sequences of all protein constructs used in this study can be found in the source data in Supplementary Data 1.

Plasmid transformation into *H. volcanii*

The genetic system of the *H. volcanii* parent strain (H26) we were using is based on a PyrE selection marker that causes uracil auxotrophy[26]. Plasmids that were transformed into *H. volcanii* were first passed through a *dam−/dcm− E. coli* strain. To transform *H. volcanii*, polyethylene glycol 600 (PEG 600) was used[26]. Cells were grown to an optical density (OD_{600}) of 0.8 in 10 ml and collected (3,000g, 10 min). The pellet was washed in 2 ml buffered spheroplast solution (1 M NaCl, 27 mM KCl, 50 mM Tris-HCl and 15% w/v sucrose, set to a pH of 8.5 after components were dissolved) and then resuspended in 600 µl buffered spheroplasting solution. For 1 transformation, 200 µl of the prepared cell suspension was used. For spheroplast formation, 50 mM EDTA (pH 8.0) was added and the cells were incubated for 10 min at room temperature. Unmethylated plasmids (1 µg) were mixed with 83 mM EDTA and made up to a total volume of 30 µl with unbuffered spheroplasting solution (1 M NaCl, 27 mM KCl and 15 % w/v sucrose). After 10 min, DNA was added to the cells and the tube was gently inverted for mixing. Five minutes later, 250 µl 60% PEG 600 was added, the cells were gently mixed and then incubated for 30 min. Next, 1.5 ml of spheroplast dilution solution (23% saltwater, 15% w/v sucrose and 3.75 mM CaCl2) was added and the cells were collected at 3,000g for 8 min. Subsequently, the cell pellet was collected at the bottom of the tubes and 1 ml of regeneration solution (18% saltwater, 1× YPC, 15% w/v sucrose and 3.75 mM CaCl2) was added to the undissolved pellet. The pellet was incubated for 1.5 h at 45 °C, dissolved by tapping the tube and then incubated for another 3.5 h. Next, cells were collected (3,000g, 8 min) and resuspended in 1 ml transformant dilution solution (18% saltwater, 15% w/v sucrose and 3 mM CaCl2). Transformed cells (100 µl) were plated on selective Ca plates or Ca plates supplemented with 0.5 mM tryptophan if required.

Construction of the CdpB1 depletion strain

For the generation of a tryptophan-inducible allele of *cdpB1*, integrative plasmid pSVA13510 was transformed into *H. volcanii* strain H98 (Δ*pyrE*, Δ*hdrB*). To check for correct upstream integration and correct orientation of the construct, transformants were screened via colony PCR. One colony with the correct insertion was then transferred to 5 ml YPC medium and grown overnight to induce the pop-out of the integrative plasmid. The next day the culture was diluted 1:500 into fresh YPC medium and grown overnight. This process was repeated once more to ensure pop-out of all integrated plasmids. To select for pop-out events, 100 µl of cells diluted by 10^{-1}, 10^{-2} and 10^{-3} were plated on Ca plates; supplemented with 50 µg ml^{-1} 5-fluoroorotic acid (5-FOA), 0.09 mM uracil and 0.5 mM tryptophan; and incubated at 45 °C until colonies were visible. Colonies were then picked and transferred to a Ca plate supplemented with uracil and 0.5 mM tryptophan. Subsequently, grown colonies were transferred using blotting paper onto a Ca-uracil plate. Four colonies that showed limited growth on the plate without tryptophan were screened via colony PCR for the correct mutation. The PCR product of one colony was sequenced and successful promoter exchange was confirmed.

Construction of the CdpB2 and CdpB3 deletion strain

For the generation of the deletion strains, either plasmid pSVA13521 (*cdpB2* deletion plasmid) or pSVA13522 (*cdpB3* deletion plasmid) were transformed into *H. volcanii* strain H26. One colony per knockout attempt was picked and transferred into 5 ml YPC medium to induce pop-out of the plasmid as described above. Pop-out cultures were plated in the same dilution as above on Ca plates supplemented with 50 µg ml^{-1} 5-FOA and 0.09 mM uracil. Possible knockout colonies were transferred to non-selective YPC plates and screened via colony PCR after growth. Successful gene deletions were confirmed by sequencing. The *cdpB2/B3* double-deletion strain was constructed by transforming pSVA13523 in the *cdpB2* deletion strain, following the steps described above.

Spot survival assay

To find the best tryptophan concentration for the CdpB1 depletion strain to grow, a spot dilution assay was performed with Ca plates containing 0.45 mM uracil and varying tryptophan concentrations (0 mM, 0.25 mM, 0.5 mM, 0.75 mM, 1 mM and 1.25 mM). The pre-culture was grown in YPC medium overnight at 45 °C. The next day the culture was diluted to an OD_{600} of 0.2, and a serial dilution up to 10^{-5} was prepared. From each dilution, 5 µl was spotted on the plate. The strain H26 was included as a control. Plates were sealed in a plastic bag and incubated for 3–4 days at 45 °C. Viability of the *cdpB2*, *cdpB3* and *cdpB2/B3* deletion strains was tested with Ca plates with no additional uracil. To overcome the uracil auxotrophy, the deletion strains and the control were transformed with empty expression vector pTA1392 complementing the *pyrE* deletion. Pre-cultures were grown in Cab medium and treated as the CdpB1 depletion strain the next day. Spot dilution assays to check for the functionality of CdpB1−mNeonGreen and CdpB2−mNeonGreen were performed as described for the deletion strains.

Microscopy and image analysis

To investigate the cellular localizations of proteins in the wild-type or mutant strains, phase contrast and fluorescence light microscopy was used. *H. volcanii* cells were transformed with expression plasmids and pre-cultures of the transformants grown in 5 ml Cab medium. The next day cells were diluted in 20 ml Cab medium and grown until they reached an OD_{600} of 0.03. To immobilize cells, they were spotted on a 0.3% w/v agarose pad containing 18% saltwater (144 g l^{-1}

NaCl, 18 g l^{-1} MgCl$_2$·6H$_2$O, 21 g l^{-1} MgSO$_4$·7H$_2$O, 4.2 g l^{-1} KCl and 12 mM Tris·HCl, pH 7.5). When the samples dried, cells were covered with a coverslip and observed with an inverted microscope (Zeiss Axio Observer.Z1, controlled via Zeiss Blue v.3.3.89). The integrity of the mNeonGreen fusion constructs were assessed by western blotting using an antibody against mNeonGreen (mNeonGreen Tag (E8E3V) rabbit monoclonal antibody number 55074; 1:1,000 dilution; Cell Signaling Technology) and a secondary antibody (goat anti-rabbit IgG (H + L) secondary antibody, HRP number 65-6120; 1:10,000 dilution; Invitrogen) for signal detection. Cells expressing the respective constructs were grown to an OD$_{600}$ of 0.1, collected and resuspended to a theoretical OD$_{600}$ of 10 in phosphate-buffered saline supplemented with 2.5 mM MgCl$_2$ and DNase I (1 mg ml^{-1}). To fully lyse the cells, 0.1% v/v dodecyl-β-D-maltoside (DDM) was added and the cells were incubated on ice for 10 min. To remove cell debris, the lysate was centrifuged at 13,000g for 5 min at 4 °C. A volume of 10 µl per cell lysate of each construct was loaded on 15% SDS gels and subsequently analysed by western blotting.

To investigate the effect of the modifications and perturbations on cell shapes, pre-cultures of the deletion strains and H26, transformed with empty plasmid pTA1392 to complement the uracil auxotrophy, were grown in 5 ml Cab medium at 45 °C. The next day cells were diluted in 20 ml fresh Cab medium with uracil and again grown overnight. Samples were taken at different growth stages, starting at an OD$_{600}$ of 0.01, and the last sample was taken at an OD$_{600}$ of 3.6. Cells were imaged on agarose pads as previously described.

To image the SepF depletion strain, HTQ239 transformed with different expression plasmids cells were grown in 20 ml Cab medium, supplemented with 1 mM tryptophan, to an OD$_{600}$ of 0.02. To induce SepF depletion, the cells were collected (3,000g, 10 min) and resuspended in pre-warmed Cab medium. Cells were directly imaged after resuspension and 3 h, 6 h, 9 h and 24 h after the start of depletion.

The CdpB1 depletion strain transformed with different plasmids was grown in Cab medium, supplemented with 0.5 mM tryptophan. As the tryptophan promotor was not strong enough to bring the viability of the CdpB1 depletion strain back to wild-type levels, cells grew constantly with reduced CdpB1 levels and a transfer of the cells into medium devoid of tryptophan was not necessary to induce CdpB1 depletion. As cells were constantly depleted of CdpB1, only samples from one time point were taken.

Overnight microscopy was performed using the CellASIC ONIX2 microfluidic system and B04A-03 plates. Channels were primed with medium for 10 min under constant flow at 34.5 kPa. For cell loading, overnight cultures were diluted back to an OD$_{600}$ of 0.05 and flowed for 15 s into the chamber at 13.8 kPa. Cells were imaged for 16 h at 45 °C under a constant flow of fresh medium at 5 kPa.

To analyse cell shapes and the areas of the signals, FIJI (v.1.54b)[30] and the MicrobeJ (v.5.13l)[31] plug-in were used. The area of each individual signal per cell was measured.

Heterologous expression and purification of *A. fulgidus* CdpB1, CdpB2 and SepF

For protein production, the *E. coli* Rosetta strain was used. Cells were transformed either with pSVA13585 (His–SUMO–CdpB1), pSVA13586 (His–SUMO–CdpB2) or pSVA13587 (His–SUMO–SepF) and grown in LB medium, supplemented with kanamycin, overnight. The next day cells were diluted back to an OD$_{600}$ of 0.05 in 2 l fresh LB medium containing kanamycin and grown at 37 °C. When the cells reached an OD$_{600}$ of 0.5, protein expression was induced by addition of 0.5 mM β-D-1-thiogalactopyranoside (IPTG). Growth was continued for 3 h at 37 °C and subsequently cells were collected (6,000g for 20 min) at 4 °C. The cell pellets were immediately frozen in liquid nitrogen and stored at −80 °C

For purifications, cell pellets were resuspended in 20 ml buffer A (300 mM NaCl, 10 mM imidazole and 50 mM Na$_2$HPO$_4$, adjusted with NaH$_2$PO$_4$ to pH 8.0) and lysed by passing the cells 4× through a French press at 1,000 psi. Subsequently, cell lysates were cleared by centrifugation for 10 min at 8,000g (SS-34 rotor; Sorvall). To remove *E. coli* proteins, the cell lysates were then incubated at 70 °C for 20 min under constant shaking, and the precipitated proteins were removed by centrifugation at 4 °C for 10 min at 14,000g. A final centrifugation step at 83,540g for 45 min at 4 °C was performed before the cleared cell lysates were loaded on a 5 ml HisTrap HP column (Cytiva), which was previously equilibrated using buffer A. The column was then connected to an Äkta purifier (Cytiva) operated with the Unicorn software (v.5.11). To remove unbound samples, the column was washed with buffer B (300 mM NaCl, 20 mM imidazole and 50 mM Na$_2$HPO$_4$, pH 8.0) until absorbance at 280 nm was low and stable. For protein elution, buffer C (300 mM NaCl, 250 mM imidazole and 50 mM Na$_2$HPO$_4$, adjusted with NaH$_2$PO$_4$ to pH 8.0) was applied with a constant flow rate of 0.5 ml min^{-1}. Samples from each purification step were loaded onto 15% SDS–PAGE gels for analysis. Elution fractions were combined, 2 mM dithiothreitol (DTT) and 0.1% NP-40 was added and everything was incubated overnight at 4 °C with 2.5 µg ml^{-1} SUMO protease (expressed from pCDB302 and purified as previously described[32]). The next day the sample was loaded on a Superdex 75 26/600 column (Cytiva), equilibrated with buffer D (150 mM NaCl and 25 mM Tris–HCl, pH 8.0) and run at a constant flow rate of 0.75 ml min^{-1}. Elution fractions were combined, concentrated by Amicon Ultra Centrifugal Filters (10 kDa cut-off; Merck Millipore) and the protein concentration was determined (BCA Assay Makro Kit; Serva). Purified proteins were frozen in liquid nitrogen and stored at −80 °C until use.

Oligomeric state of CdpB1/B2 and complex formation with SepF

To determine the oligomeric state of the CdpB proteins, 50 µM of each protein was loaded on a Superdex 75 10/300 column (Cytiva), equilibrated with buffer D (150 mM NaCl and 25 mM Tris–HCl, pH 8.0). Elution was for 30 min at a constant flow rate of 0.5 ml min^{-1}. To investigate complex formation, CdpB1, CdpB2 and SepF proteins were mixed in the following combinations: CdpB1 and SepF; CdpB2 and SepF; CdpB1 and CdpB2; and CdpB1, CdpB2 and SepF (each at 50 µM). The mixtures were then incubated for 10 min at room temperature, before they were loaded onto a Superdex 75 26/60 column (Cytiva) operated with buffer D as described above. Elution fractions of the single- and multi-protein runs were collected, concentrated via Amicon Ultra Centrifugal Filters (10 kDa cut-off; Merck Millipore) and applied on 10–20% gradient SDS–PAGE gels.

Crystallization of the *A. fulgidus* CdpB1/B2 complex

To obtain a stochiometric CdpB1–CdpB2 protein complex, purified proteins were mixed at a molar ratio of 1:2 (CdpB1:CdpB2) and loaded onto a Superose 6 Increase 10/300 GL SEC column (Cytiva). The column was equilibrated in 25 mM Tris-HCl, 150 mM NaCl, 5 mM MgCl$_2$ and 1 mM TCEP, pH 8.0. Gel filtration fractions containing the CdpB1–CdpB2 complex were pooled and concentrated using Vivaspin Turbo 5 kDa centrifugal concentrators (Sartorius). Initial crystallization hits were obtained using our in-house crystallization facility[33]. Crystals were grown at 19 °C by sitting-drop vapour diffusion. Crystals were obtained in 200 nl drops composed of 100 nl crystallization reservoir solution (5% MPD, 0.04 M MgCl$_2$ and 0.05 M sodium cacodylate, pH 6.0) and 100 nl protein solution at 10 mg ml^{-1}. Crystals were collected, cryo-protected with 30% (v/v) glycerol in the reservoir solution and flash frozen in liquid nitrogen.

Crystal structure determination

Diffraction data were collected at Diamond Light Source on beamline I24 at 100 K and processed with AutoPROC[34] (XDS, built 10 January 2022; Pointless, 1.12.13; Aimless, 0.7.8; CCP4, 8.0.001; STARANISO: 2.3.87 (18 May 2022)). Anisotropic diffraction limits were applied using

the online server STARANISO[35]. The structure of CdpB1–CdpB2 was solved by molecular replacement with Phaser[36], using an AlphaFold2 prediction of CdpB1 monomer as the template[37,38]. Interactive model building was performed with Coot[39], refinement with REFMAC5 (ref. [40]) and phenix.refine[41], and validation with Molprobity[42]. Crystallographic data and model statistics are summarized in Supplementary Table 3. Figures of atomic models were prepared with PyMOL[43].

Pyrococcus furiosus liposome preparation
Lipids were isolated from 1 g of freeze-dried *P. furiosus* cells using soxhlet extraction as described in ref. [44]. Instead of chloroform, dichloromethane was used. *P. furiosus* lipids (12 mg) were placed into a round-bottomed glass vial (part number 5183-2075; Agilent Technologies) and mixed with 500 μl of chloroform. Once the lipids were dissolved, the mixture was left overnight in the glass vial to allow the chloroform to fully evaporate. The residual solvent was removed using a glass vacuum desiccator for 3–5 hours, which produced a thin film of solid lipid mixture. The lipid film and 20 mM Tris-HCl (pH 7.4) buffer were separately heated to 37 °C. The buffer (150 μl) was then added to the film and shaken vigorously for 3 h at 37 °C. The liposome suspension was loaded into a gas-tight syringe (1,000 ml; SKU, 610017-1Ea; Avanti) and passed through a 0.2 μm Whatman membrane filter several times using a hand-driven Avanti mini-extruder. The liposome suspension was used immediately.

Electron microscopy
For single-particle electron microscopy analysis, *A. fulgidus* SepF, CdpB1 and CdpB2 proteins were individually purified as described. Proteins were mixed in a ratio of 1:1:1 to overall concentrations of 0.5–1 mg ml⁻¹ and then incubated for 15 min at room temperature. After incubation, the sample containing the SepF–CdpB1–CdpB2 complex was gently mixed with 0.05% of octyl-β-glucoside (B2007; Melford). UltrAuFoil R 2/2 Au 200 grids (MD-AGS188-2; Molecular Dimensions) were glow discharged using an Edwards Sputter Coater S150B at 0.2 mbar for 10 s. The sample (6 μl) was loaded into glow-discharged electron microscopy grids, back blotted and plunge frozen using a custom-made manual plunger.

To prepare the SepF, SepF–CdpB1 and SepF–CdpB1–CdpB2 complexes for incubation with *Pyrococcus* liposomes, the proteins were buffer exchanged using Zeba Spin Desalting Columns (89882; Thermo Scientific) into buffer containing 25 mM Tris-HCl, 50 mM NaCl and 5 mM MgCl₂, pH 7.4. The SepF–CdpB1–CdpB2 complex was prepared by mixing proteins in a 1:1:1 ratio to a final concentration of 1 mg ml⁻¹. All other samples were also at a concentration of 1 mg ml⁻¹ and at a stoichiometric ratio of 1:1, where applicable. Samples were incubated for 15 min at room temperature before mixing with liposomes in a 1:1 (c/c) ratio. After 10 s incubation with liposomes, 6 μl of each sample was applied to glow-discharged UltrAuFoil R 2/2 Au 200 grids (MD-AGS188-2; Molecular Dimensions), back blotted and plunge frozen using a custom-made manual plunger.

Cryo-EM data collection
Cryo-EM data were collected using a Titan Krios G3 microscope (Thermo Fisher Scientific) operated at 300 kV and equipped with a BioQuantum energy filter (Gatan) with a slit width of 20 eV. The images were collected with a post-GIF K3 direct electron detector (Gatan) operating in super-resolution mode, at a magnification corresponding to a pixel size of 0.826 Å. The dose rate was set to 19 e– per pixel per second and a total dose of 50 e– per Å² was fractionated over 50 frames. Data were collected using EPU software (v.3.4.0) with a defocus range of −1 μm to −2.5 μm. A total of 8,180 micrographs were collected.

Cryo-EM data processing and structure determination
The dataset was processed in RELION 4.0 (ref. [45]). Videos were motion corrected and CTF estimated in RELION. Approximately 500 particles were manually picked from a random selection of micrographs

for automated picking. A total of ~800,000 particles were picked and extracted into boxes 259 Å wide. After several rounds of 2-dimensional classification, which resulted in ~68,000 very good particles, an initial 3-dimensional model was generated in cryoSPARC v.4 (ref. [46]). Three-dimensional auto-refinement using C2 symmetry and post-processing in RELION v.4 yielded a map at a 5.1 Å resolution that was easily rigid-body fitted with the atomic model obtained using crystallography (CdpB1 and CdpB2) and AlphaFold2 (SepF) containing a dimer of a CdpB2–CdpB1–SepF–SepF–CdpB1–CdpB2 complex. Given the confirmatory nature of the cryo-EM structure, no further processing was attempted.

Heterologous expression and purification of *H. volcanii* CdpB1, CdpB2, SepF and FtsZ2
All *H. volcanii* proteins (SepF, FtsZ2, CdpB1 and CdpB2) were constructed with His–SUMO N-terminal fusion and expressed in *E. coli* BL21 (DE3) for 3 h at 37 °C in LB medium supplemented with 100 μg ml⁻¹ ampicillin, in the presence of 1 mM IPTG, after reaching an OD₆₀₀ 0.6–0.8. Cells were pelleted at 6,000g for 45 min, resuspended in the supernatant, centrifuged again at 4,000g for 30 min, and finally flash frozen using liquid nitrogen and then stored at −80 °C. Cells were thawed and resuspended in lysis buffer (100 mM HEPES, pH 7.4, 150 mM KCl, 20 mM imidazole and 1 mM DTT) supplemented with EDTA-free protease inhibitor tablets (1 per 50 ml buffer) and 1 mg ml⁻¹ DNase I. The lysis was performed using a Q700 sonicator equipped with a probe of 12.7 mm diameter immersed into the resuspended pellet. The sonication was done for 10 min (amplitude 40, on time 1 s, off time 4 s). Next, the cell debris was removed by centrifugation at 31,000g for 45 min, and the cleared lysate was incubated with HisPur Ni-NTA resin (Thermo Fisher Scientific) for 1 h. Subsequently, the resin was washed with lysis buffer (30 column volumes) and His–SUMO-tagged protein eluted with an imidazole gradient elution buffer (100 mM HEPES, pH 7.4, 150 mM KCl, 100–400 mM imidazole and 1 mM DTT). Fractions were further analysed by SDS–PAGE, pooled and dialysed overnight against the storage buffer (100 mM HEPES, pH 7.4, 150 mM KCl, 10% glycerol and 1 mM DTT) in the presence of His–Ulp1 protease (1:100 molar ratio) for His–SUMO cleavage. To remove the cleaved His–SUMO tag and His–Ulp1, reverse affinity chromatography was performed using Protino Ni-IDA resin (LACTAN Macherey Nagel). After 30 min of incubation with the resin, flow-through was collected and analysed by SDS–PAGE. At this point, SepF, FtsZ2 and CdpB2 were aliquoted, flash frozen in liquid nitrogen and stored at −80 °C. CdpB1 was loaded onto a HiLoad 16/600 Superdex 75 size exclusion column pre-equilibrated with storage buffer and run over the column via an Äkta purifier (Cytiva) operated with the Unicorn software (v.7). Fractions were pooled, flash frozen in liquid nitrogen and stored at −80 °C. All steps were done at 4 °C and concentrations of all proteins were determined by Bio-Rad Protein Assay Dye Reagent Concentrate.

SEC coupled with multi-angle light scattering
Individual proteins and protein complexes were resolved on a Superdex 200 Increase 10/300 (Cytiva) with a flow rate of 0.5 ml min⁻¹ in high salt buffer (1 M KCl, 10 mM MgCl₂ and 100 mM HEPES, pH 7.4) coupled with a miniDAWN light-scattering device (Wyatt) at room temperature. The peak areas were defined based on the changes in refractive index, which was used to determine molecular mass. The analysis was done using ASTRA software (Wyatt). Individual proteins SepF, CdpB1 and CdpB2 were run at 0.9 mg ml⁻¹, 0.7 mg ml⁻¹ and 0.5 mg ml⁻¹, respectively. When two proteins were pre-mixed, the concentration of each protein was 0.25 mg ml⁻¹, whereas all three proteins were pre-mixed at a concentration of 17 mg ml⁻¹ per protein.

Pelleting assay for recruitment of CdpB1 and CdpB2 by SepF
Chloroform solutions of lipids (DOPC:DOPG:DOGS-NTA-Ni ratio of 66%:33%:1%) were dried under the nitrogen stream until a lipid film

was formed. The lipid film was solubilized with the swelling buffer (100 mM HEPES, pH 7.4, 1 M sucrose and 5 mM $MgCl_2$), incubated for 30 min at 37 °C and vortexed extensively to make the multi-lamellar vesicle mixture homogeneous. Next, protein mixtures or proteins alone were diluted in reaction buffer (100 mM HEPES, pH 7.4, 1 M KCl and 5 mM $MgCl_2$) to 10 μM. Both protein and vesicle solutions were mixed in a 1:1 ratio, incubated for 20 min at room temperature and centrifuged at 21,000*g*. Supernatant and pellets were analysed on 4–20% pre-cast SDS–PAGE gels. In these assays, we used 6×His–SepF (from pMK18), Cy5–CdpB1 (from pMK60) and CF488–CdpB2 (from pMK61), which were purified the same way as native proteins (see above). The rationale behind using these constructs is the following: 6×His–SepF was used to be able to bind to the membrane through the interaction with Ni-NTA-containing lipids; as both CdpB1 and CdpB2 are very small proteins, on the gels they are usually covered by the vesicles and hence we used labelled versions of these proteins to be able to see if the proteins were present in the pellet samples.

Pelleting assay for the interaction of SepF with FtsZ2

The vesicles and proteins were prepared in the same way as previously described. As FtsZ2 was non-specifically binding to the Ni-NTA-containing lipids, we used a His–SUMO protein to passivate the vesicles before starting the experiment. FtsZ2 and 6×His–SepF were used at a final concentration of 5 μM.

Mass photometry assay for CdpB1 and CdpB2

Glass coverslips for mass photometry experiments were prepared by washing them in water, isopropanol and then water again for 15 min each in a sonicator bath. The coverslips were air dried and pre-cast chambers were attached to them. The final concentration of the proteins was 10 nM in the reaction buffer (100 mM HEPES, pH 7.4, 1 M KCl and 5 mM $MgCl_2$) and the samples were imaged on a Refeyn Mass Photometer 2 for 1 min.

Homology searches and sequences analysis

For homology searches, we assembled a local databank of 3,661 archaeal genomes (see source data in Supplementary Data 1), representatives of all major phyla available in public databases as of January 2022. We carried out HMM-based homology searches using the pfam domains PF05239, PF18822, PF12327 and PF04472 corresponding to the PRC, CdvA, FtsZ and SepF domains, respectively. We used hmmsearch from the HMMER3.3.2 package[47] and set the threshold-to-noise cut-offs using the option cut_nc. Several rounds of curation were performed to discard false positives, using additional information such as domain organization, alignments and phylogeny. In the Asgardarchaeota and TACK groups, some CdvA homologues also matched with the PRC domain. However, given the absence of FtsZ and the specific presence of CdvA in these groups, we annotated these sequences as CdvA. Taxonomic distribution was mapped onto a schematic tree of Archaea based on ref. 48 using IToL[49].

Shortening of the article during editorial revision was done with the help of ChatGPT (v.4).

Reporting summary

Further information on research design is available in the Nature Portfolio Reporting Summary linked to this article.

Data availability

The data that support the findings of this study are available in the Source Data. Source data are provided with this paper. Coordinates have been submitted to the Protein Data Bank (PDB) with accession code 8QZO.

References

1. Mahone, C. R. & Goley, E. D. Bacterial cell division at a glance. *J. Cell Sci.* **133**, jcs237057 (2020).

2. Andrade, V. & Echard, A. Mechanics and regulation of cytokinetic abscission. *Front. Cell Dev. Biol.* **10**, 1046617 (2022).

3. Makarova, K. S., Yutin, N., Bell, S. D. & Koonin, E. V. Evolution of diverse cell division and vesicle formation systems in Archaea. *Nat. Rev. Microbiol.* **8**, 731–741 (2010).

4. Ithurbide, S., Gribaldo, S., Albers, S.-V. & Pende, N. Spotlight on FtsZ-based cell division in Archaea. *Trends Microbiol.* **30**, 665–678 (2022).

5. Makarova, K. S. & Koonin, E. V. Two new families of the FtsZ-tubulin protein superfamily implicated in membrane remodeling in diverse bacteria and archaea. *Biol. Direct* **5**, 33 (2010).

6. Liao, Y., Ithurbide, S., Evenhuis, C., Löwe, J. & Duggin, I. G. Cell division in the archaeon *Haloferax volcanii* relies on two FtsZ proteins with distinct functions in division ring assembly and constriction. *Nat. Microbiol.* **6**, 594–605 (2021).

7. Pende, N. et al. SepF is the FtsZ-anchor in archaea, with features of an ancestral cell division system. *Nat. Commun.* https://doi.org/10.1038/s41467-021-23099-8 (2021).

8. Nußbaum, P., Gerstner, M., Dingethal, M., Erb, C. & Albers, S. V. The archaeal protein SepF is essential for cell division in *Haloferax volcanii*. *Nat. Commun.* **12**, 3469 (2021).

9. Anantharaman, V. & Aravind, L. The PRC-barrel: a widespread, conserved domain shared by photosynthetic reaction center subunits and proteins of RNA metabolism. *Genome Biol.* **3**, RESEARCH0061 (2002).

10. Patro, M., Duggin, I. G., Albers, S.-V. & Ithurbide, S. Influence of plasmids, selection markers and auxotrophic mutations on Haloferax volcanii cell shape plasticity. *Front. Microbiol.* **14**, 1270665 (2023).

11. Li, Z. et al. Positioning of the motility machinery in halophilic Archaea. *mBio* **10**, e00377-19 (2019).

12. Ye, H. et al. Crystal structure of the putative adapter protein MTH1859. *J. Struct. Biol.* **148**, 251–256 (2004).

13. Król, E. et al. Bacillus subtilis SepF binds to the C terminus of FtsZ. *PLoS ONE* **7**, e43293 (2012).

14. Sogues, A. et al. Essential dynamic interdependence of FtsZ and SepF for Z-ring and septum formation in *Corynebacterium glutamicum*. *Nat. Commun.* **11**, 1641 (2020).

15. Elkins, J. G. et al. A korarchaeal genome reveals insights into the evolution of the Archaea. *Proc. Natl Acad. Sci. USA* **105**, 8102–8107 (2008).

16. Duman, R. et al. Structural and genetic analyses reveal the protein SepF as a new membrane anchor for the Z ring. *Proc. Natl Acad. Sci. USA* **110**, E4601–E4610 (2013).

17. Wenzel, M. et al. Control of septum thickness by the curvature of SepF polymers. *Proc. Natl Acad. Sci. USA* **118**, e2002635118 (2021).

18. Du, S. & Lutkenhaus, J. Assembly and activation of the *Escherichia coli* divisome. *Mol. Microbiol.* **105**, 177–187 (2017).

19. Errington, J. & Wu, L. J. in *Prokaryotic Cytoskeletons* (eds Löwe, J. & Amos, L. A.) 67–101 (Springer, 2017); https://doi.org/10.1007/978-3-319-53047-5_3

20. Abdul-Halim, M. F. et al. Lipid anchoring of archaeosortase substrates and mid-cell growth in Haloarchaea. *mBio* **11**, 863746 (2020).

21. Blanch Jover, A. & Dekker, C. The archaeal Cdv cell division system. *Trends Microbiol.* https://doi.org/10.1016/j.tim.2022.12.006 (2023).

22. Moriscot, C. et al. Crenarchaeal CdvA forms double-helical filaments containing DNA and interacts with ESCRT-III-Like CdvB. *PLoS ONE* **6**, e21921 (2011).

23. Samson, R. Y. et al. Molecular and structural basis of ESCRT-III recruitment to membranes during archaeal cell division. *Mol. Cell* **41**, 186–196 (2011).

24. Zhao, S. et al. Widespread PRC barrel proteins are necessary for haloarchaeal cell division. *Nat Microbiol.* https://doi.org/10.1038/s41564-024-01615-y (2024).

25. Bertani, G. Studies on lysogenesis. I. The mode of phage liberation by lysogenic *Escherichia coli*. *J. Bacteriol.* **62**, 293–300 (1951).

26. Allers, T., Ngo, H.-P., Mevarech, M. & Lloyd, R. G. Development of additional selectable markers for the halophilic Archaeon *Haloferax volcanii* based on the leuB and trpA genes. *Appl. Environ. Microbiol.* **70**, 943–953 (2004).

27. de Silva, R. T. et al. Improved growth and morphological plasticity of *Haloferax volcanii*. *Microbiology* **167**, 001012 (2021).

28. Watson, J. F. & García-Nafría, J. In vivo DNA assembly using common laboratory bacteria: a re-emerging tool to simplify molecular cloning. *J. Biol. Chem.* **294**, 15271–15281 (2019).

29. Braun, F. et al. Cyclic nucleotides in archaea: cyclic di-AMP in the archaeon *Haloferax volcanii* and its putative role. *MicrobiologyOpen* **8**, e00829 (2019).

30. Schindelin, J. et al. Fiji: an open-source platform for biological-image analysis. *Nat. Methods* **9**, 676–682 (2012).

31. Ducret, A., Quardokus, E. M. & Brun, Y. V. MicrobeJ, a tool for high throughput bacterial cell detection and quantitative analysis. *Nat. Microbiol.* **1**, 16077 (2016).

32. Lau, Y.-T. K. et al. Discovery and engineering of enhanced SUMO protease enzymes. *J. Biol. Chem.* **293**, 13224–13233 (2018).

33. Gorrec, F. & Löwe, J. Automated protocols for macromolecular crystallization at the MRC Laboratory of Molecular Biology. *J. Vis. Exp.* https://doi.org/10.3791/55790 (2018).

34. Vonrhein, C. et al. Data processing and analysis with the autoPROC toolbox. *Acta Crystallogr. D* **67**, 293–302 (2011).

35. Vonrhein, C. et al. Advances in automated data analysis and processing within autoPROC, combined with improved characterisation, mitigation and visualisation of the anisotropy of diffraction limits using STARANISO. *Acta Crystallogr. A* **74**, a360–a360 (2018).

36. McCoy, A. J., Grosse-Kunstleve, R. W., Storoni, L. C. & Read, R. J. Likelihood-enhanced fast translation functions. *Acta Crystallogr. D* **61**, 458–464 (2005).

37. Jumper, J. et al. Highly accurate protein structure prediction with AlphaFold. *Nature* **596**, 583–589 (2021).

38. Varadi, M. et al. AlphaFold protein structure database: massively expanding the structural coverage of protein-sequence space with high-accuracy models. *Nucleic Acids Res.* **50**, D439–D444 (2022).

39. Emsley, P., Lohkamp, B., Scott, W. G. & Cowtan, K. Features and development of Coot. *Acta Crystallogr. D* **66**, 486–501 (2010).

40. Murshudov, G. N., Vagin, A. A. & Dodson, E. J. Refinement of macromolecular structures by the maximum-likelihood method. *Acta Crystallogr. D* **53**, 240–255 (1997).

41. Liebschner, D. et al. Macromolecular structure determination using X-rays, neutrons and electrons: recent developments in Phenix. *Acta Crystallogr. D* **75**, 861–877 (2019).

42. Chen, V. B. et al. MolProbity: all-atom structure validation for macromolecular crystallography. *Acta Crystallogr. D* **66**, 12–21 (2010).

43. Schrödinger, L. & DeLano, W. The PyMOL Molecular Graphics System (Delano Scientific, 2020).

44. Albers, S. V., Konings, W. N. & Driessen, A. J. in *Methods in Microbiology: Extremophiles*, Vol. 35 (eds Rainey, F. A. & Oren, A.) 161–171 (Academic Press, 2006).

45. Scheres, S. H. W. A Bayesian view on Cryo-EM structure determination. *J. Mol. Biol.* **415**, 406–418 (2012).

46. Punjani, A., Rubinstein, J. L., Fleet, D. J. & Brubaker, M. A. cryoSPARC: algorithms for rapid unsupervised cryo-EM structure determination. *Nat. Methods* **14**, 290–296 (2017).

47. Johnson, L. S., Eddy, S. R. & Portugaly, E. Hidden Markov model speed heuristic and iterative HMM search procedure. *BMC Bioinf.* **11**, 431 (2010).

48. Garcia, P. S., Gribaldo, S. & Borrel, G. Diversity and evolution of methane-related pathways in Archaea. *Annu. Rev. Microbiol.* **76**, 727–755 (2022).

49. Letunic, I. & Bork, P. Interactive Tree Of Life (iTOL) v.4: recent updates and new developments. *Nucleic Acids Res.* **47**, W256–W259 (2019).

Acknowledgements

Author contributions

Competing interests

The authors declare no competing interests.

Additional information

Supplementary information The online version contains supplementary material available at https://doi.org/10.1038/s41564-024-01600-5.

Correspondence and requests for materials should be addressed to Sonja-Verena Albers.

Peer review information *Nature Microbiology* thanks Daniela Barilla, William Margolin and the other, anonymous, reviewer(s) for their contribution to the peer review of this work.

Reprints and permissions information is available at www.nature.com/reprints.

nature portfolio

Corresponding author(s): Sonja-Verena Albers

Last updated by author(s): Dec 22, 2023

Reporting Summary

Nature Portfolio wishes to improve the reproducibility of the work that we publish. This form provides structure for consistency and transparency in reporting. For further information on Nature Portfolio policies, see our Editorial Policies and the Editorial Policy Checklist.

Statistics

For all statistical analyses, confirm that the following items are present in the figure legend, table legend, main text, or Methods section.

n/a	Confirmed	
☐	☒	The exact sample size (*n*) for each experimental group/condition, given as a discrete number and unit of measurement
☐	☒	A statement on whether measurements were taken from distinct samples or whether the same sample was measured repeatedly
☒	☐	The statistical test(s) used AND whether they are one- or two-sided *Only common tests should be described solely by name; describe more complex techniques in the Methods section.*
☒	☐	A description of all covariates tested
☒	☐	A description of any assumptions or corrections, such as tests of normality and adjustment for multiple comparisons
☐	☒	A full description of the statistical parameters including central tendency (e.g. means) or other basic estimates (e.g. regression coefficient) AND variation (e.g. standard deviation) or associated estimates of uncertainty (e.g. confidence intervals)
☒	☐	For null hypothesis testing, the test statistic (e.g. *F*, *t*, *r*) with confidence intervals, effect sizes, degrees of freedom and *P* value noted *Give P values as exact values whenever suitable.*
☒	☐	For Bayesian analysis, information on the choice of priors and Markov chain Monte Carlo settings
☒	☐	For hierarchical and complex designs, identification of the appropriate level for tests and full reporting of outcomes
☒	☐	Estimates of effect sizes (e.g. Cohen's *d*, Pearson's *r*), indicating how they were calculated

Our web collection on statistics for biologists contains articles on many of the points above.

Software and code

Policy information about availability of computer code

Data collection	Zeiss Blue 3.3.89 was used to acquire microscopy pictures; Protein alignment was done using Jalview Version 2.11.0 with MUSCLE (default settings); Unicorn (Version 5.11) was used for protein purification and size exclusion chromatography of the A. fulgidus proteins; Unicorn (Version 7) was used for protein purification and SEC of the H. volcanii proteins; homology searches were performed using HMMER (Version 3.3.2); Cryo-EM data were collected with EPU software (Version 3.4.0)
Data analysis	Fiji (Version 1.54b) with MicrobeJ plug-in (Version5.13l) was used for analysis of microscopy Data and partially generation of graphs; Microsoft Excel 2013 and Graphpad Prism (Version 6.07) was used for, Microscopy Data (co-localization, cell size analysis) and size exclusion chromatography profiles; Astra Software (Version 7.3.2.21) was used for SEC-MALS data; crystalization Data were processed with AutoPROC (XDS: BUILT 20220110; POINTLESS: 1.12.13; AIMLESS: 0.7.8; CCP4: 8.0.001; STARANISO: 2.3.87 (20220518)); PyMOL (Version 2.5) was used for figures of atomic models; Cryo-EM data were processed with cryoSPARC (Version 4) and RELION (Version 4); phylogenetic tree was assembled with iTOL (Version 6); CorelDraw X5 was used to make the model and assemble figures

For manuscripts utilizing custom algorithms or software that are central to the research but not yet described in published literature, software must be made available to editors and reviewers. We strongly encourage code deposition in a community repository (e.g. GitHub). See the Nature Portfolio guidelines for submitting code & software for further information.

Data

Policy information about [availability of data](#)

All manuscripts must include a [data availability statement](#). This statement should provide the following information, where applicable:
- Accession codes, unique identifiers, or web links for publicly available datasets
- A description of any restrictions on data availability
- For clinical datasets or third party data, please ensure that the statement adheres to our [policy](#)

> The data that support the findings of this study are available from the corresponding author upon request. Source data are provided with this paper.

Human research participants

Policy information about [studies involving human research participants and Sex and Gender in Research.](#)

Reporting on sex and gender	N/A
Population characteristics	N/A
Recruitment	N/A
Ethics oversight	N/A

Note that full information on the approval of the study protocol must also be provided in the manuscript.

Field-specific reporting

Please select the one below that is the best fit for your research. If you are not sure, read the appropriate sections before making your selection.

☒ Life sciences   ☐ Behavioural & social sciences   ☐ Ecological, evolutionary & environmental sciences

For a reference copy of the document with all sections, see [nature.com/documents/nr-reporting-summary-flat.pdf](#)

Life sciences study design

All studies must disclose on these points even when the disclosure is negative.

Sample size	No statistical methods were used to predetermine sample size. Sample sizes were chosen based on historical data.
Data exclusions	Fig.1 b/d, Supplementary Fig.2 b/d/e/f : only cells with both GFP and mCherry signal were used for analysis and extreme outliers (misspositioning of the fluorescence maxima compared to app. 99% of the other maxima) compared to the rest of the data were removed Fig.2 c/f, Supplementary Fig. 8 b/d/e: extreme outliers (extremly increased signal areas; e.g. whole cell shows a fluorescence signal) compared to the rest of the data of each strain were removed Supplementary Fig. 10 b/c/d the first 34 min of the elution were removed from the graph since the proteins of interest eluted afterwards Supplementary Fig. 10 e the first 32 min of the elution were removed from the graph since the proteins of interest eluted afterwards
Replication	Each experiment was at least performed in three biological replicates. All replication attempts were successful.
Randomization	Respective strains for different experiments were selected randomly for inoculation from plate. They were grown under similar conditions and were therefore equivalent at the start of experiments. Their differences observed can be attributed to the genotype or treatment under testing conditions.
Blinding	No blinding was performed as this was not necessary for our study. Strains were grown under similar conditions and were therefore equivalent at the start of experiments. Their differences observed can be attributed to the genotype or treatment under testing conditions.

Reporting for specific materials, systems and methods

We require information from authors about some types of materials, experimental systems and methods used in many studies. Here, indicate whether each material, system or method listed is relevant to your study. If you are not sure if a list item applies to your research, read the appropriate section before selecting a response.

Materials & experimental systems

n/a	Involved in the study
☐	☒ Antibodies
☒	☐ Eukaryotic cell lines
☒	☐ Palaeontology and archaeology
☒	☐ Animals and other organisms
☒	☐ Clinical data
☒	☐ Dual use research of concern

Methods

n/a	Involved in the study
☒	☐ ChIP-seq
☒	☐ Flow cytometry
☒	☐ MRI-based neuroimaging

Antibodies

Antibodies used

1. mNeonGreen Tag (E8E3V) Rabbit mAb #55074 (Cell Signaling Technology) (1:1000 dilution)
2. Goat anti-Rabbit IgG (H+L) Secondary Antibody, HRP #65-6120 (invitrogen) (1:10000 dilution)

Validation

Validation was based on technical data sheets provided by the manufacturer. Specifity statement by the manufacturer: mNeonGreen Tag (E8E3V) Rabbit mAb detects recombinant proteins containing mNeonGreen protein. The antibody recognizes mNeonGreen protein fused to either the amino or carboxy terminus of targeted proteins in transfected cells. mNeonGreen Tag (E8E3V) Rabbit mAb detects exogenously expressed mNeonGreen protein in cells expressed under a CMV promoter. Expression under other promoters has not been evaluated. This antibody does not cross-react with green fluorescent protein (GFP).
Functionality of the antibody was validated through the manufacturer by Western-Blotting: Western blot analysis of extracts from 293T cells, untransfected (-) or transfected with amino-terminal or carboxy-terminal mNeonGreen Tag fusion protein (+), using mNeonGreen Tag (E8E3V) Rabbit mAb (upper) or β-Actin (D6A8) Rabbit mAb #8457 (lower)
andConfocal immunofluorescent analysis of mNeonGreen-transfected HCT 116 cells, fixed with either 4% formaldehyde (top) or 100% methanol (bottom), using mNeonGreen Tag (E8E3V) Rabbit mAb (red) and DAPI #4083 (blue). Note: methanol fixation reduces the innate fluorescence of mNeonGreen, but not the binding of E8E3V.